Vehicle System Dynamics, Vol. 25, pp. 251-276, 1996

Speed Tracking and Vehicle Follower Control Design for Heavy-Duty Vehicles*

DIANA YANAKIEV† and IOANNIS KANELLAKOPOULOS‡

SUMMARY

In this paper we address the problem of automation of heavy-duty vehicles. After a brief description of the dynamic model used in our design and simulations, we develop nonlinear controllers with adaptation, first for speed control and then for vehicle follower longitudinal control. We consider both autonomous operation as well as intervehicle communication, and evaluate the stability and performance properties of our controllers in several different scenarios through analysis and simulation.

1. INTRODUCTION

Advanced Vehicle Control Systems (AVCS) are critical components of Intelligent Transportation Systems (ITS). They incorporate both longitudinal and lateral schemes for semi- or fully automated vehicle operation, aimed at increasing highway traffic flow, with improved fuel efficiency and enhanced safety. While a multitude of results exist for control of passenger cars [3, 9, 15, 20], heavy-duty commercial vehicles have been largely ignored so far, with the exception of the results reported in [4]. In this paper we present the first results on adaptive longitudinal control design for heavy vehicles.

As part of this effort we are developing realistic models which capture all the important characteristics of the longitudinal vehicle dynamics. Our first modeling task was the development of a turbocharged (TC) diesel engine model suitable for vehicle control which is briefly presented in Section 2. The engine model is then combined with the automatic transmission, drivetrain and brake models to obtain a longitudinal heavy-duty vehicle model. Section 2 also contains a linearization-based analysis of the longitudinal vehicle

*This research was supported in part by CalTrans through PATH MOU 124 and in part by NSF through Grants ECS-9309402 and ECS-9502945.

†Graduate Student, Department of Electrical Engineering, UCLA, Los Angeles, CA 90095-1594, USA.

‡Assistant Professor, Department of Electrical Engineering, UCLA, Los Angeles, CA 90095-1594, USA.

model, which provides useful information regarding the significance of each state for the longitudinal behavior of the vehicle. In Section 3 we develop two nonlinear control schemes for speed tracking. The performance of the designed fixed-gain PIQD and adaptive PIQ controllers is evaluated on the basis of simulation results. Existing PID and adaptive PI speed controllers are also applied to our longitudinal truck model for the sake of comparison. Then, in Section 4, we design an adaptive nonlinear controller for vehicle following which can operate in both autonomous mode (AICC) and cooperative mode with intervehicle communication (platooning). The single-vehicle stability properties of this controller are proven via Lyapunov analysis, while its string stability and transient performance properties under several scenarios are evaluated through simulation. Finally, we present our conclusions in Section 5.

2. LONGITUDINAL TRUCK MODEL

The longitudinal model of a truck is shown in Figure 1. The Engine module contains the TC diesel engine model. The four gear automatic transmission model is included in the Transmission block. The longitudinal dynamics equations are in the Chassis module.

2.1. Turbocharged (TC) diesel engine model

The vast majority of existing internal combustion engine models serve purposes such as engine performance improvement or diagnostics. Engine models suitable for vehicle control have been developed only for normally aspirated spark ignition (SI) engines. Unfortunately, they cannot be adapted to describe the compression ignition (CI) of the diesel engine and to capture the effect of the turbocharger.

Using several TC diesel engine modeling techniques available in the literature [7, 8, 10, 11, 14, 19], we have compiled a model consisting of three differential and several algebraic equations, as well as four 2-D maps, which are compiled from experimental data available in the literature. Our model is based on the *mean torque production* model developed by Kao and Moskwa [12]. The modeled engine is turbocharged and intercooled, has six cylinders and $0.014\,\mathrm{m}^3$ (14 liters) displacement volume. The block diagram in Figure 2 gives an overview of the model structure.

As in the SI engine model developed by Cho and Hedrick [3, 15], two of the states are the *intake manifold (IM) pressure* and the *engine speed*. However, due to the different fueling method, the fueling lag is not considered here. In the diesel engine, the fuel is injected directly into the cylinder immediately before the combustion takes place. This eliminates the need to account for the fueling dynamics. The *TC rotor speed* is another state which needs to be introduced due to the presence of the turbocharger.

The equation for the IM pressure p_{im} has been derived by differentiating

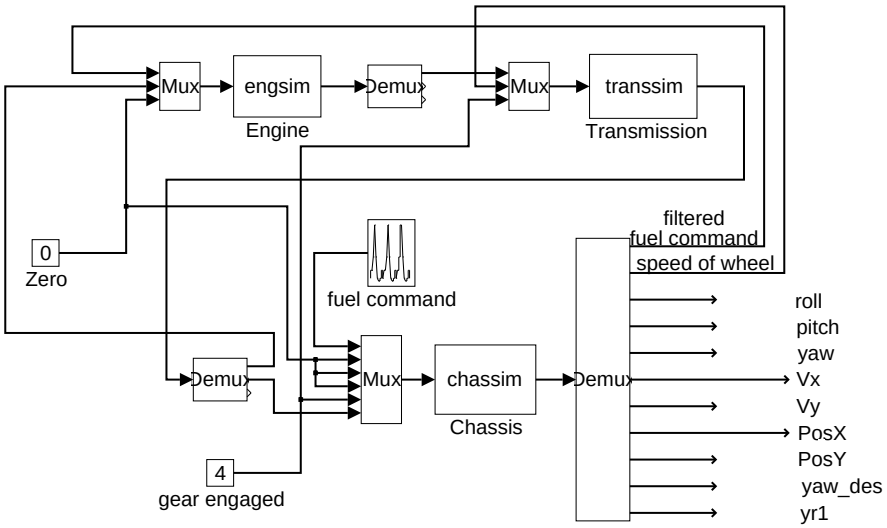

Input to Engine:	fuel command load torque unused	Output From Engine:	rpm net torque unused
Input to Trans:	rpm speed of wheel gear engaged	Ouput from Trans:	load torque driving torque unused
Input to Chassis:	commanded fuel commanded steering commanded brake road curvature gear engaged driving torque		

Figure 1: Truck longitudinal model.

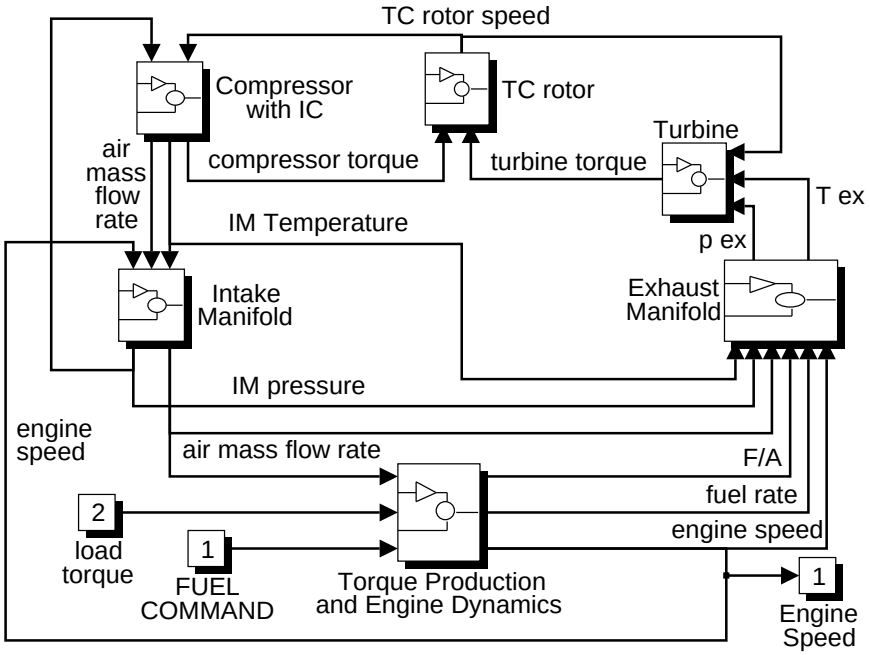

Figure 2: TC diesel engine model representation.

the ideal gas law:

$$\dot{p}_{\rm im} + \frac{\eta_{\rm v} V_{\rm d} N_{\rm e}}{120 V_{\rm im}} p_{\rm im} = \dot{m}_{\rm c} \frac{R T_{\rm im}}{V_{\rm im}} \ , \tag{2.1}$$

where $T_{\rm im}$ and $V_{\rm im}$ are respectively the IM temperature and volume, $\eta_{\rm v}$ is the volumetric efficiency, $V_{\rm d}$ is the displacement volume of the engine, $N_{\rm e}$ is the engine speed in revolutions per minute (rpm)—so that $N_{\rm e} = \omega_{\rm e} \frac{60}{2\pi}$, where $\omega_{\rm e}$ is the engine speed in rad/s—and $\dot{m}_{\rm c}$ is the compressor air mass flow rate.

The engine speed ω_e is obtained by integrating the angular acceleration of the crankshaft, which is determined from Newton's second law:

$$M_{\rm ind}(t - \tau_{\rm i}) - M_{\rm f}(t) - M_{\rm load}(t) = J_{\rm e} \dot{\omega}_{\rm e}(t) \, . \tag{2.2}$$

In the above equation, $M_{\rm ind}$ is the indicated torque and $M_{\rm f}$ the friction torque of the engine, $M_{\rm load}$ is the load torque which is determined by the transmission and the drivetrain subsystems of the vehicle model, and $J_{\rm e}$ is the effective inertia of the engine. The *production delay* $\tau_{\rm i}$ represents the average difference between the time of issuing a command to change the indicated engine torque and the time when the injection valve can be operated. These events are determined by the position of the crankshaft angle. Therefore, the production delay and all other delays associated with this model have constant values measured in crankshaft angle. Converted in seconds, they become inversely proportional to the engine speed.

The TC dynamic equation is also derived using Newton's second law:

$$M_{\rm t} - M_{\rm c} = J_{\rm tc} \dot{\omega}_{\rm tc} \, , \tag{2.3}$$

where $M_{\rm t}$ is the torque provided by the turbine, $M_{\rm c}$ is the torque absorbed by the compressor, and $J_{\rm tc}$ is the effective inertia of the turbocharger. Integration of the TC angular acceleration $\dot{\omega}_{\rm tc}$ yields the TC rotor speed $\omega_{\rm tc}$.

Some intermediate computations are necessary to determine the other variables participating in the state equations. Steady-state empirical characteristics and experimental data in the form of 2-D maps, as well as algebraic relations are used, in addition to the state equations, to obtain a complete mathematical description of the system.[1]

2.2. Torque converter

Our automatic transmission model is based on the assumptions that gear shifting is instantaneous and that there is no torsion in the driveline. The static nonlinear torque converter model derived by Kotwicki [13] has been employed. This model is well suited for vehicle modeling because it provides explicit terminal relations between torques and speeds. Experimentally justified approximation of the exact detailed expressions yields the following

[1] For a detailed description of our engine and transmission model, the reader is referred to the report [21].

representation of the pump torque M_{P} and the turbine torque M_{T} as functions of the pump speed $\omega_{\mathrm{P}} = \omega_{\mathrm{e}}$ and the turbine speed ω_{T}:

$$M_{\mathrm{P}} = \alpha_0\omega_{\mathrm{P}}^2 + \alpha_1\omega_{\mathrm{P}}\omega_{\mathrm{T}} + \alpha_2\omega_{\mathrm{T}}^2 \tag{2.4}$$

$$M_{\mathrm{T}} = \beta_0\omega_{\mathrm{P}}^2 + \beta_1\omega_{\mathrm{P}}\omega_{\mathrm{T}} + \beta_2\omega_{\mathrm{T}}^2. \tag{2.5}$$

The coefficients $\alpha_0, \alpha_1, \alpha_2, \beta_0, \beta_1, \beta_2$ are obtained by regression from experimental data. Although the form of the equations is preserved in both modes of operation, different coefficients have to be determined for the regions when the engine is driving the vehicle and vice versa. The pump and turbine angular velocities are compared to determine the current operating region. The respective coefficients are then used to compute the pump torque, which is the load torque applied to the engine, and the turbine torque, which is the shaft torque transmitted to the drivetrain.

2.3. Transmission mechanicals

The assumption that there is no torsion in the driveline establishes a direct relationship between the angular velocity of the torque converter turbine ω_{t} and that of the vehicle's driving wheels ω_{w}:

$$\omega_{\mathrm{w}} = R_{\mathrm{total}}\,\omega_{\mathrm{T}} = R_i\,R_{\mathrm{d}}\,\omega_{\mathrm{T}}\,, \tag{2.6}$$

where R_i is the reduction ratio of the ith gear range and R_{d} is the final drive reduction ratio. The model is further simplified by the instantaneous gear shifting assumption, eliminating the need for an additional state which appears during shifting.

2.4. Longitudinal drivetrain equations

The angular velocity of the driving wheels is determined by the torque converter turbine torque M_{T}, the tractive tire torque $F_{\mathrm{t}}h_{\mathrm{w}}$, where F_{t} is the tractive tire force and h_{w} is the static ground-to-axle height of the driving wheels, and the braking torque M_{b}:

$$J_{\mathrm{w}}\,\dot{\omega}_{\mathrm{w}} = \frac{M_{\mathrm{T}}}{R_{\mathrm{total}}} - F_{\mathrm{t}}h_{\mathrm{w}} - M_{\mathrm{b}}\,, \tag{2.7}$$

where J_{w} is the lumped inertia of the wheels.

Currently, the brake actuating system is represented via a first-order linear system with a time constant τ_{b}, i.e., the braking torque M_{b} is obtained from

$$\dot{M_{\mathrm{b}}} = \frac{M_{\mathrm{bc}} - M_{\mathrm{b}}}{\tau_{\mathrm{b}}}\,, \tag{2.8}$$

where M_{bc} is the commanded braking torque. This is only a crude approximation of the complicated brake dynamics present in heavy-duty vehicles, but

it is fairly reasonable for longitudinal control. A more detailed brake model is currently under development.

The tractive force F_t depends linearly on the tire slip up to approximately 15% slip. Since the tire slip is always positive, it is defined as:

$$i_\mathrm{d} = 1 - \frac{v}{h_\mathrm{w}\,\omega_\mathrm{w}} \quad \text{or} \quad i_\mathrm{b} = 1 - \frac{h_\mathrm{w}\,\omega_\mathrm{w}}{v}\,, \tag{2.9}$$

where v is the vehicle velocity, depending on whether the tire is under driving torque ($F_\mathrm{t} = k_i\, i_\mathrm{d}$) or under braking torque ($F_\mathrm{t} = -k_i\, i_\mathrm{b}$).

The aerodynamic drag force F_a and the force generated by the rolling resistance of the tires ($F_\mathrm{r} = \frac{M_\mathrm{r}}{h_\mathrm{w}}$) have to be subtracted from the tractive force to yield the force that accelerates or decelerates the vehicle. The state equation for the truck velocity becomes:

$$\dot{v} = \frac{F_\mathrm{t} - F_\mathrm{a} - F_\mathrm{r}}{m}\,, \tag{2.10}$$

where the vehicle mass is denoted by m. The force F_a is determined from the aerodynamic drag coefficient c_a and the vehicle speed:

$$F_\mathrm{a} = c_\mathrm{a}\, v^2\,. \tag{2.11}$$

The rolling resistance torque $M_\mathrm{r} = F_\mathrm{r}\, h_\mathrm{w}$ is a linear function of the vehicle mass:

$$M_\mathrm{r} = c_\mathrm{r}\, m\, g\,. \tag{2.12}$$

Substituting (2.11) and (2.12) into (2.10), we obtain:

$$\dot{v} = \frac{F_\mathrm{t} - c_\mathrm{a}\, v^2}{m} - \frac{c_\mathrm{r}\, g}{h_\mathrm{w}}\,. \tag{2.13}$$

Finally, a first-order filter with a time constant τ_f is also included in the vehicle model to account for the dynamics of the fuel pump and the actuators which transmit the fuel command u to the injectors:

$$\dot{u}_\mathrm{f} = \frac{1}{\tau_\mathrm{f}}\,(-u_\mathrm{f} + u)\,. \tag{2.14}$$

The variable u_f is a scaled version of the index[2] Y. The minimum index necessary to maintain idle speed corresponds to $u_\mathrm{f}^{\min} = 3$ and the maximum index corresponds to $u_\mathrm{f}^{\max} = 85$.

2.5. Linearization of the longitudinal model

The resulting longitudinal vehicle model described so far is highly nonlinear and detailed enough to capture all the important characteristics of the dynamic behavior of a heavy-duty vehicle. However, it is far too complex to be

[2]The index Y is defined as the position of the fuel pump rack, which determines the amount of fuel provided for combustion.

used as the basis for control design. Due to the presence of several implicit algebraic relations and empirical 2-D maps, it is virtually impossible to obtain a state-space model in a form that is useful for control design. Instead, the model was linearized around several operating points determined by different fuel command/vehicle mass combinations. The results showed that the sixth-order linearized model has the same number of dominant modes throughout the examined range, albeit with significant variations in individual parameter values. The modes associated with the angular velocity of the wheel and the fuel system (cf. (2.14)) are always very fast compared to the remaining ones, and can thus be ignored. Of the remaining four modes, those associated with the IM pressure, the engine speed and the TC rotor speed are much faster than the mode corresponding to the vehicle velocity.

Thus, the longitudinal truck model relating the vehicle speed to the fuel command input can be reduced to a first-order linear model:

$$\frac{\delta v}{\delta u} = \frac{b}{s+a} \ , \tag{2.15}$$

where the values of b and a depend on the operating point, i.e., on the steady state values of the vehicle speed and the load torque. This reduced-order linearized model is the starting point for the design of our control schemes. However, this does not imply that our modeling effort was wasted, since our simulations are always carried out using the full nonlinear model. What this order reduction and linearization do imply is that our controllers do not rely on the particular details of the vehicle model and are thus inherently robust to modeling uncertainties. They are also easier to implement, since they do not contain highly complicated algebraic or dynamic equations. The price paid for this simplicity and robustness is that we can only achieve good performance if the required maneuvers are slower than the slowest neglected modes. But since here we are only interested in maneuvers with time constants of several seconds, this limitation does not play a significant role.

3. CONTROL DESIGN FOR SPEED TRACKING

Most longitudinal control schemes available in the literature use separate controllers for throttle and brake control. This creates the need for an additional supervisory layer, which uses *ad hoc* rules to determine which controller should be active at any given time. In contrast, our adaptive nonlinear controller is versatile enough to handle both fuel and brake, thus eliminating the undesirable overhead associated with switching between different controllers.

When the output of the controller is positive a fuel command is issued, while negative output activates the brakes. To deal with the different actuator limits, the controller output is multiplied with a fixed gain whenever it is negative. To avoid chattering between fuel and brake, a hysteresis element is

included in the controller.[3]

In this section we consider the problem of *speed tracking*. Two nonlinear controllers are designed: One with fixed gains and an adaptive one whose gains are continuously adjusted. Their performance is compared through simulations which use the nonlinear truck model of the previous section.

3.1. PIQD with anti-windup

We begin with the ubiquitous PID controller with an implementable approximate derivative term and an anti-windup scheme to reduce speed overshoot. In speed tracking, overshoot is much more undesirable than undershoot because of passenger comfort considerations. It is even more undesirable in a vehicle-following scenario, where it may lead to collisions. Since overshoot is usually associated with high-gain control, one way of reducing it would be to reduce the control gains. However, this would result in longer response times. To allow fast compensation of large tracking errors without the need for high gains, we introduce a signed quadratic (Q) term into the PID controller. As we will see, our resulting nonlinear PIQD controller outperforms conventional PID controllers over a wide operating region. The PIQD control law is:

$$u = -k_{\rm p} e_v - k_{\rm i} \frac{1}{s} \left\{ e_v - \frac{1}{T_{\rm t}} \left[u - {\rm sat}(u) \right] \right\} - k_{\rm q} e_v |e_v| - k_{\rm d} \frac{\tau_{\rm d} s}{\frac{1}{N}\tau_{\rm d} s + 1} e_v \,, \quad (3.1)$$

where ${\rm sat}(\cdot)$ is an appropriately defined saturation function that reflects the physical limits of the controller, and $e_v = v - v_{\rm d}$ is the error between the actual vehicle speed v and its desired value $v_{\rm d}$. The latter is obtained by passing the commanded speed $v_{\rm c}$ through a first-order filter to eliminate discontinuities and provide a smoother response:

$$\dot{v}_{\rm d} = -v_{\rm d} + v_{\rm c} \,. \quad (3.2)$$

3.2. Adaptive PIQ controller

There are several reasons for including adaptation in our control design. Even if a controller is perfectly tuned for some operating region, it is likely to demonstrate inferior performance in other conditions due to the severe nonlinearities present in the system. A gain scheduling approach could be successful in overcoming the disadvantages of a fixed gain controller, but it would require extensive a priori information. Another reason is that adaptation makes the control design much less dependent on the specific vehicle. Keeping in mind the prospective application of AVCS to a large variety of road vehicles, the latter consideration becomes even more significant.

Let us now consider the linearized model from (2.15), where the linearization is performed around the desired speed $v_{\rm d}$. Denoting by $e_v = v - v_{\rm d}$ the

[3] While this gain and hysteresis can be viewed as switching logic, they are far less complicated than the rules required in systems that use separate controllers for fuel and brake.

deviation of the speed from its desired value $v_{\rm d}$, we obtain the model:

$$\dot{e}_v = \dot{v} - \dot{v}_{\rm d} = -a\, e_v + b\,(u - u_{\rm d}) + d_0\,, \tag{3.3}$$

where $u_{\rm d}$ is the (unknown) nominal value of the control corresponding to the desired speed $v_{\rm d}$, and the disturbance term d_0 includes the external disturbances as well as the effect of the neglected fast modes.

We propose the adaptive PIQ control law:

$$u = -\hat{k}_1\, e_v - \hat{k}_2 - \hat{k}_3\, e_v\, |e_v|\,, \tag{3.4}$$

where $\hat{k}_1$, $\hat{k}_2$, $\hat{k}_3$ are time-varying parameters continuously adjusted by an update law. The adaptive coefficient $\hat{k}_2$ represents the integral term of the controller as we shall see below. Substituting equation (3.4) into equation (3.3) yields:

$$\dot{v} = -(a + b\hat{k}_1)e_v - b\hat{k}_2 - b\hat{k}_3\, e_v\, |e_v| + d\,, \tag{3.5}$$

where the new disturbance term

$$d = d_0 - bu_{\rm d} + \dot{v}_{\rm d} \tag{3.6}$$

also includes the unknown nominal value of the control and the time variation of the desired speed. Next, we adopt the *nonlinear* reference model:

$$\dot{v}_{\rm m} = -a_{\rm m}(v_{\rm m} - v_{\rm d}) - q_{\rm m}(v_{\rm m} - v_{\rm d})|e_v|\,, \tag{3.7}$$

where $a_{\rm m} > 0$ and $q_{\rm m} \geq 0$. If a, b, and d were constant and known, the values of k_1, k_2, and k_3 satisfying the model reference control objective would be computed as

$$\begin{aligned} a + bk_1 &= a_{\rm m} \\ bk_2 &= d \\ bk_3 &= q_{\rm m}\,. \end{aligned} \tag{3.8}$$

Since the parameters of the plant are unknown, we replace k_1, k_2, and k_3 by their estimates in the control law (3.4). To design update laws for these estimates, we use the tracking error $e_{\rm r} = v - v_{\rm m}$, computed from (3.5)–(3.8) as

$$\dot{e}_{\rm r} = \dot{v} - \dot{v}_{\rm m} = -a_{\rm m}e_{\rm r} - q_{\rm m}|e_v|e_{\rm r} + b(\tilde{k}_1 e_v + \tilde{k}_2 + \tilde{k}_3 e_v|e_v|)\,, \tag{3.9}$$

where $\tilde{k}_i = k_i - \hat{k}_i$, $i = 1, 2, 3$, are the parameter errors.

Then, the update laws are obtained via the partial Lyapunov function:[4]

$$V = \frac{e_{\rm r}^2}{2} + b\frac{\tilde{k}_1^2}{2\gamma_1} + b\frac{\tilde{k}_2^2}{2\gamma_2} + b\frac{\tilde{k}_3^2}{2\gamma_3}\,, \tag{3.10}$$

[4]This Lyapunov function is called partial because it does not include the states $v_{\rm m}$ and $v_{\rm d}$ which are part of our controller dynamics.

where γ_1, γ_2, γ_3 are positive design constants and b is unknown but positive. The choices

$$\begin{aligned} \dot{\hat{k}}_1 &= \text{Proj}\left[\gamma_1 e_{\text{r}} e_v\right] \\ \dot{\hat{k}}_2 &= \text{Proj}\left[\gamma_2 e_{\text{r}}\right] \\ \dot{\hat{k}}_3 &= \text{Proj}\left[\gamma_3 e_{\text{r}} e_v |e_v|\right], \end{aligned} \tag{3.11}$$

where $\text{Proj}[\cdot]$ is the projection operator to a compact interval containing the true value of the parameter, yield

$$\dot{V} \leq -a_{\text{m}} e_{\text{r}}^2 - q_{\text{m}} |e_v| e_{\text{r}}^2 . \tag{3.12}$$

This guarantees the boundedness of e_{r}, $\hat{k}_1$, $\hat{k}_2$, and $\hat{k}_3$. From (3.2) we know that v_{d} and $\dot{v}_{\text{d}}$ are bounded and that $v_{\text{d}} - v_{\text{c}} \to 0$, $\dot{v}_{\text{d}} \to 0$ as $t \to \infty$. Then, (3.7) implies that $v_{\text{m}} - v_{\text{d}} \to 0$, $\dot{v}_{\text{m}} \to 0$. Combining these with the boundedness of e_{r}, $\hat{k}_1$, $\hat{k}_2$, and $\hat{k}_3$, we see that all the states of our closed-loop system are bounded, and so are their derivatives. Then, from (3.12) we conclude that $e_{\text{r}} = v - v_{\text{m}} \to 0$. Coupled with $v_{\text{m}} - v_{\text{d}} \to 0$ and $v_{\text{d}} - v_{\text{c}} \to 0$, this implies that our speed tracking objective is achieved:

$$\lim_{t\to\infty} [v(t) - v_{\text{m}}(t)] = \lim_{t\to\infty} [v(t) - v_{\text{d}}(t)] = \lim_{t\to\infty} [v(t) - v_{\text{c}}(t)] = 0 .$$

From (3.11) we see that the $\hat{k}_2$-term in (3.4) is indeed an "integral" term, since it is the integral of the error e_{r}. This term compensates the effects of external disturbances such as road grades and headwinds, and it also contains the estimate of u_{d}, the nominal control value. We should also note that the reason for using parameter projection in (3.11) is to guarantee *a priori* that the parameter estimates remain bounded. This is a necessary robustness modification since our reduced-order model is perturbed by external disturbances and unmodeled dynamics which can, in general, result in unbounded parameter estimates.

3.3. Comparative simulations

In order to compare the performance of our two nonlinear controllers (fixed-gain PIQD and adaptive PIQ) to each other and to more conventional linear controllers (fixed-gain PID and adaptive PI), we simulated the corresponding closed-loop systems of all four controllers using the same staircase profile for the commanded vehicle speed. The comparison results between fixed-gain PID and PIQD controller, both with anti-windup, are shown in Figure 3 and between adaptive PI and PIQ controller in Figure 4. In both cases, the inclusion of the nonlinear Q term in the control law results in better tracking of the desired speed. However, in the fixed-gain case, the improvement is more pronounced. While some overshoot is observed with the PID (despite the

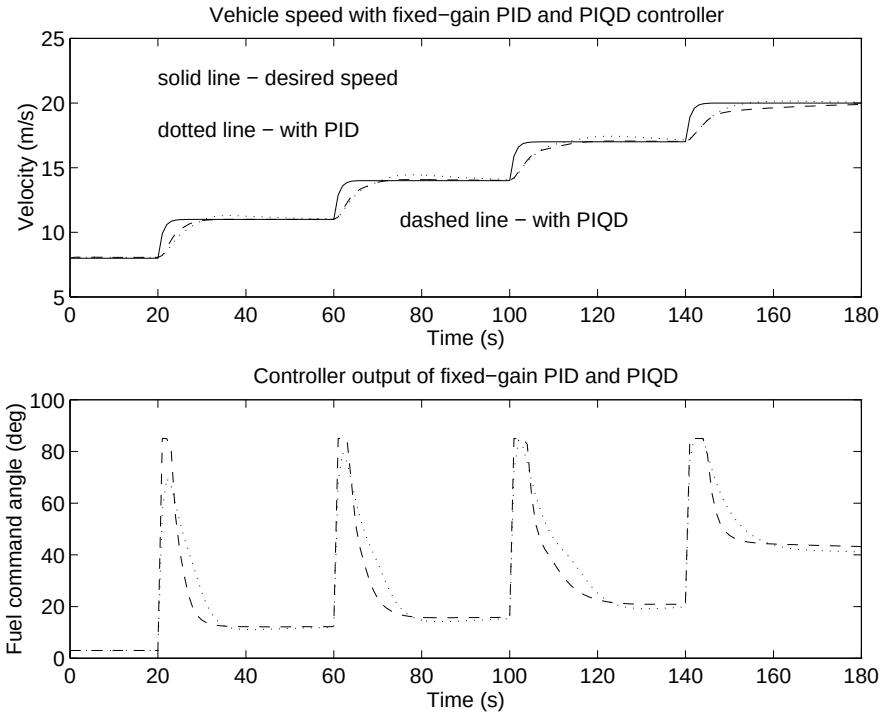

Figure 3: Vehicle speed with PID and PIQD control in response to a commanded staircase profile.

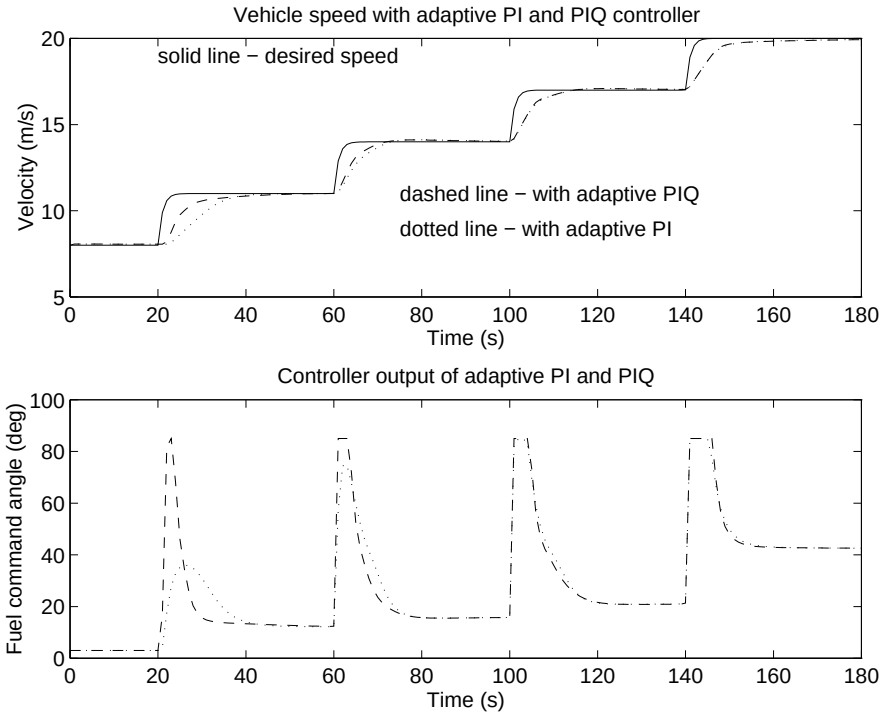

Figure 4: Vehicle speed with adaptive PI and adaptive PIQ control in response to a commanded staircase profile.

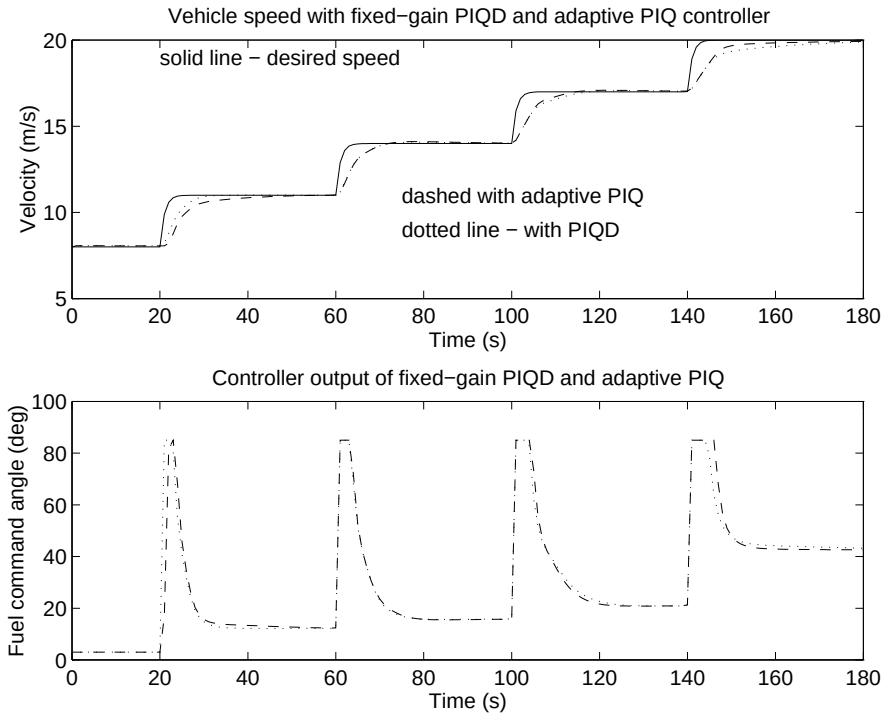

Figure 5: Performance comparison of PIQD and adaptive PIQ control.

use of anti-windup), the PIQD overcomes this problem. Both adaptive controllers track the desired speed without overshoot. However, the performance of the adaptive PIQ controller is much more uniform for different operating conditions.

The fixed-gain PIQD and the adaptive PIQ are compared in Figure 5. The advantage of the adaptive controller is that due to adaptation it provides more uniform tracking of the desired speed over a wider range of operating conditions.

From the plotted outputs of all simulated controllers we see that aggressive control action is necessary for good tracking of step increases in the commanded speed. This confirms our intuitive expectation that more aggressive controllers are needed to overcome the considerably lower actuation-to-weight ratio of a heavy truck compared to a passenger car. However, simply increasing the gains of a linear controller would cause larger overshoot. Here we avoided this problem with the inclusion of the nonlinear Q term. Finally, we point out that the usual disadvantage of passenger discomfort due to aggressive control action is much less pronounced in heavy vehicles due to their

larger mass, which results in significantly lower acceleration and jerk profiles than in passenger cars.

4. CONTROL DESIGN FOR VEHICLE FOLLOWING

The continuous demand for increasing the traffic capacity of highway systems has so far been met by expansion of existing highways and construction of new ones. However, these solutions are quickly becoming infeasible in many large metropolitan areas. A widely proposed strategy for effectively increasing highway throughput without expansion [17, 6, 16, 18] is to group automatically controlled vehicles in tightly spaced formations called *platoons*. Platooning provides significantly higher traffic throughput when combined with small intervehicle spacing. The control design for platoons has to guarantee not only the desired performance for individual vehicles but also for the whole formation. One of the key issues here is *string stability*, which ensures that errors decrease in magnitude as they are propagated upstream, thus eliminating the undesirable "slinky effect" associated with heavy traffic patterns. The fact that string stability cannot be achieved for platoons with *constant intervehicle spacing* under autonomous operation has been known for more than twenty years [5, 17]. String stability can be guaranteed if the lead vehicle is transmitting its velocity [17] or velocity and acceleration [16] to all other vehicles in the platoon. This approach yields stable platoons with small intervehicle spacings at the cost of introducing and maintaining continuous intervehicle communication. String stability can also be recovered in autonomous operation if a *speed-dependent* spacing policy is adopted, which incorporates a *fixed time headway* term in addition to the constant distance [5, 2]. This approach avoids the communication overhead, but results in larger spacings between adjacent vehicles and thus in longer platoons, thereby yielding smaller increases in traffic throughput.

In this section we design an adaptive nonlinear controller which can operate both autonomously as well as with intervehicle communication. The quantities of interest between any two adjacent platoon members are defined in Figure 6. In the speed tracking case the primary issue addressed in the control design is regulating the difference between the actual and the desired velocity. In the vehicle-following scenario this would correspond to regulating the relative velocity $v_{\mathrm{r}} = v_{\mathrm{l}} - v_{\mathrm{f}}$, where v_{l} is the leading vehicle's velocity and can be viewed as the desired speed for the following vehicle, whose actual velocity is v_{f}. However, in this case the controller must also regulate the separation error

$$\delta = x_{\mathrm{r}} - s_{\mathrm{d}} \,, \tag{4.1}$$

where x_{r} is the actual and s_{d} the desired separation between two adjacent vehicles. The desired separation may be a function of the following vehicle's velocity:

$$s_{\mathrm{d}} = s_0 + h v_{\mathrm{f}} \,, \tag{4.2}$$

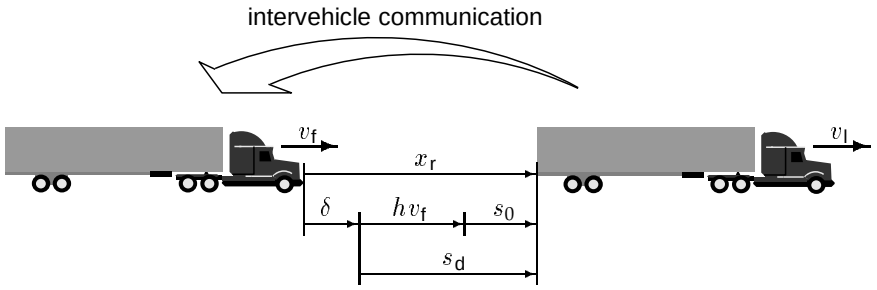

s_0 : minimum distance between vehicles
h : time headway (for speed-dependent spacing)
x_r : vehicle separation
$s_d = s_0 + hv_f$: desired vehicle separation
v_l : velocity of leading vehicle
v_f : velocity of following vehicle
$v_r = v_l - v_f$: relative vehicle velocity
$\delta = x_r - s_d$: separation error

Figure 6: Parameters of a truck platoon.

as shown in Figure 6. The parameter h is the aforementioned *time headway* and its effect is introducing more spacing at higher velocity in addition to the *fixed minimum spacing* s_0. Setting $h = 0$ results in a *constant spacing* policy.

The tasks of regulating the relative velocity and the separation error can be combined into the control objective $v_r + k\delta = 0$, where k is a positive design constant. This control objective makes sense intuitively: If two vehicles are closer than desired ($\delta < 0$) but the preceding vehicle's speed is larger than the follower's ($v_r > 0$), then the controller in the following vehicle does not need to take drastic action. The same can be said if the vehicles are farther apart than desired ($\delta > 0$) but the preceding vehicle's speed is lower than the follower's ($v_r < 0$). The selection of the coefficient k influences the response of the controller, and can be changed depending on the performance requirements. Generally, a smaller k results in improved velocity tracking at the cost of deteriorated position tracking, but the trend is not linear.

Let us now show that when our control objective is achieved, i.e., when $v_r + k\delta \equiv 0$, both the relative velocity and the separation error are regulated: $v_r \to 0$ and $\delta \to 0$. When the velocity of the lead vehicle is constant ($\dot{v}_l = 0$), we have

$$\delta = x_r - s_d = x_r - hv_f - s_0 \quad \Rightarrow \quad \dot{\delta} = v_r - h\dot{v}_f \tag{4.3}$$

$$v_r = v_l - v_f \quad \Rightarrow \quad \dot{v}_r = -\dot{v}_f\,. \tag{4.4}$$

But $v_r + k\delta \equiv 0$ implies that $\dot{v}_r + k\dot{\delta} \equiv 0$. Combining this with (4.3) and (4.4) we obtain

$$\dot{v}_r + k\,(v_r + h\dot{v}_r) \equiv 0 \;\Rightarrow\; (1+kh)\dot{v}_r + kv_r \equiv 0\,, \tag{4.5}$$

which shows that $v_r \to 0$ (since $k > 0$ and $h > 0$). From $v_r + k\delta \equiv 0$ and $v_r \to 0$ we conclude that $\delta \to 0$.

Since the control objective is to maintain $v_r + k\delta = 0$, we linearize the model around the corresponding trajectory and obtain:

$$\dot{v}_f = a(v_r + k\delta) + bu + \bar{d}\,, \tag{4.6}$$

where $\bar{d}$ again incorporates external disturbances and modeling errors, as well as the unknown nominal value of the control.

4.1. Adaptive PIQ controller

The platooning scenario is even more demanding than the speed tracking scenario in terms of fast response to accelerating and braking commands as well as various disturbances, and imposes even more stringent limits on overshoot. As a result, we focus on the adaptive PIQ scheme which in the speed tracking case proved to be the most successful in quickly reducing large errors without overshoot. Another argument for using adaptation in this case is that even if the grouped vehicles are not identical, they are expected to respond uniformly to different commands or disturbances. Hence, the fact that adaptation makes the controller response less dependent on the specific vehicle characteristics becomes more significant in the platoon case.

We propose the adaptive PIQ control law:

$$u = \hat{k}_1(v_r + k\delta) + \hat{k}_2 + \hat{k}_3\,(v_r + k\delta)\,|v_r + k\delta|\,, \tag{4.7}$$

where $\hat{k}_1$, $\hat{k}_2$, $\hat{k}_3$ are time-varying parameters which are being updated by an adaptive law. Substituting equation (4.7) into equation (4.6) yields:

$$\dot{v}_f = (a + b\hat{k}_1)(v_r + k\delta) + b\hat{k}_2 + b\hat{k}_3\,(v_r + k\delta)\,|v_r + k\delta| + \bar{d}\,. \tag{4.8}$$

To design update laws for the parameter estimates, we consider the nonlinear reference model:

$$\dot{v}_m = a_m(v_l - v_m + k\delta) + q_m(v_l - v_m + k\delta)|v_r + k\delta|\,, \tag{4.9}$$

where $a_m > 0$ and $q_m \geq 0$. If a, b, and $\bar{d}$ were known, the coefficients of the controller would be computed from (3.8) with $d = -\bar{d}$. The tracking error $e_r = v_f - v_m$ is computed from (4.8), (4.9), and (3.8):

$$\begin{aligned} \dot{e}_r = \dot{v}_f - \dot{v}_m \;\; &= \;\; -a_m e_r - q_m e_r|v_r + k\delta| \\ &\quad -b\left[\tilde{k}_1(v_r + k\delta) + \tilde{k}_2 + \tilde{k}_3(v_r + k\delta)|v_r + k\delta|\right]. \end{aligned} \tag{4.10}$$

Then

$$\begin{aligned}\dot{v}_{\rm r} &= \dot{v}_{\rm l} - \dot{v}_{\rm f} = \dot{v}_{\rm l} - \dot{e}_{\rm r} - \dot{v}_{\rm m} \\ &= \dot{v}_{\rm l} - a_{\rm m}(v_{\rm r} + k\delta) - q_{\rm m}(v_{\rm r} + k\delta)|v_{\rm r} + k\delta| \\ &\quad + b\left[\tilde{k}_1(v_{\rm r} + k\delta) + \tilde{k}_2 + \tilde{k}_3(v_{\rm r} + k\delta)|v_{\rm r} + k\delta|\right].\end{aligned} \tag{4.11}$$

Recall that

$$v_{\rm r} + k\delta = v_{\rm l} - v_{\rm f} + kx_{\rm r} - khv_{\rm f} - ks_0\,, \tag{4.12}$$

which yields

$$\dot{v}_{\rm r} + k\dot{\delta} = \dot{v}_{\rm r}(1 + kh) + kv_{\rm r} - kh\dot{v}_{\rm l}\,. \tag{4.13}$$

Let us now define the variables $x_1 = v_{\rm r}$ and $x_2 = v_{\rm r} + k\delta$. We can rewrite equations (4.11) and (4.13) and obtain the state space representation:

$$\begin{aligned}\dot{x}_1 &= -(a_{\rm m} + q_{\rm m}|x_2|)x_2 + b(\tilde{k}_1 x_2 + \tilde{k}_2 + \tilde{k}_3 x_2|x_2|) + u_1 \\ \dot{x}_2 &= kx_1 - (a_{\rm m} + q_{\rm m}|x_2|)(1 + kh)x_2 \\ &\quad + b(\tilde{k}_1 x_2 + \tilde{k}_2 + \tilde{k}_3 x_2|x_2|)(1 + kh) + u_2\,,\end{aligned} \tag{4.14}$$

where $u_1 = \dot{v}_{\rm l}$ is the leading vehicle's acceleration and $u_2 = -kh\dot{v}_{\rm l}$.

Consider the Lyapunov function:

$$V = \frac{1}{2}x^T P x + \frac{e_{\rm r}^2}{2} + b\frac{\tilde{k}_1^2}{2\gamma_1} + b\frac{\tilde{k}_2^2}{2\gamma_2} + b\frac{\tilde{k}_3^2}{2\gamma_3}\,, \tag{4.15}$$

where $P = \begin{bmatrix} p_1 & p_2 \\ p_2 & p_3 \end{bmatrix}$ is a positive definite symmetric matrix. This is a complete Lyapunov function for our closed-loop system. To see this, note that it includes the variables $v_{\rm r}$, $v_{\rm r} + k\delta$, $v_{\rm f} - v_{\rm m}$, $\tilde{k}_1$, $\tilde{k}_2$, and $\tilde{k}_3$. Since $v_{\rm l}$, k_1, k_2, and k_3 are bounded external signals, the variables in (4.15) are related via a nonsingular transformation to $v_{\rm f}$, $v_{\rm m}$, δ, $\hat{k}_1$, $\hat{k}_2$, and $\hat{k}_3$, which are all the variables of our system.

The derivative of (4.15) is

$$\begin{aligned}\dot{V} &= p_1 x_1 \dot{x}_1 + p_2 x_1 \dot{x}_2 + p_2 \dot{x}_1 x_2 + p_3 x_2 \dot{x}_2 \\ &\quad - \frac{b}{\gamma_1}\tilde{k}_1\dot{\tilde{k}}_1 - \frac{b}{\gamma_2}\tilde{k}_2\dot{\tilde{k}}_2 - \frac{b}{\gamma_3}\tilde{k}_3\dot{\tilde{k}}_3 + e_{\rm r}\dot{e}_{\rm r}\,.\end{aligned} \tag{4.16}$$

The choices $p_2 < 0$ and $p_1 = -(1 + kh)p_2$ cancel several cross-terms in (4.16). With these choices, we need $p_3 > \frac{-p_2}{1+kh}$ to guarantee the positive definiteness of P. The update laws:

$$\begin{aligned}\dot{\hat{k}}_1 &= \text{Proj}\left[\gamma_1\left\{[p_2 + p_3(1 + kh)]x_2^2 - e_{\rm r}x_2\right\}\right] \\ \dot{\hat{k}}_2 &= \text{Proj}\left[\gamma_2\left\{[p_2 + p_3(1 + kh)]x_2 - e_{\rm r}\right\}\right] \\ \dot{\hat{k}}_3 &= \text{Proj}\left[\gamma_3\left\{[p_2 + p_3(1 + kh)]x_2^2|x_2| - e_{\rm r}x_2|x_2|\right\}\right]\end{aligned} \tag{4.17}$$

yield

$$\begin{aligned}\dot{V} &\leq p_2 k x_1^2 + p_3 k x_1 x_2 - [p_2 + p_3(1+kh)](a_{\rm m} + q_{\rm m}|x_2|)x_2^2 \\ &\quad -(a_{\rm m} + q_{\rm m}|x_2|)e_{\rm r}^2 + p_2 x_1[u_2 - (1+kh)u_1] + x_2(p_2 u_1 + p_3 u_2)\,, \quad (4.18)\end{aligned}$$

Adding and subtracting $\frac{k\lambda p_3^2}{-4p_2}x_2^2$, where $\lambda > 1$ is a constant, and regrouping terms, we obtain:

$$\begin{aligned}\dot{V} &\leq -\frac{\lambda-1}{\lambda}(-p_2 k)x_1^2 - \left(\sqrt{\frac{-p_2 k}{\lambda}}x_1 - \frac{p_3}{2}\sqrt{\frac{k\lambda}{-p_2}}x_2\right)^2 \\ &\quad - \left\{[p_2 + p_3(1+kh)](a_{\rm m} + q_{\rm m}|x_2|) - \frac{k\lambda p_3^2}{-4p_2}\right\}x_2^2 \\ &\quad -(a_{\rm m} + q_{\rm m}|x_2|)e_{\rm r}^2 + p_2 x_1[u_2 - (1+kh)u_1] + x_2(p_2 u_1 + p_3 u_2)\,, \quad (4.19)\end{aligned}$$

hence

$$\begin{aligned}\dot{V} &\leq -\frac{\lambda-1}{\lambda}(-p_2 k)x_1^2 \\ &\quad - \left\{[p_2 + p_3(1+kh)](a_{\rm m} + q_{\rm m}|x_2|) - \frac{k\lambda p_3^2}{-4p_2}\right\}x_2^2 \\ &\quad -(a_{\rm m} + q_{\rm m}|x_2|)e_{\rm r}^2 + p_2 x_1[u_2 - (1+kh)u_1] + x_2(p_2 u_1 + p_3 u_2)\,. \quad (4.20)\end{aligned}$$

To guarantee that $\dot{V} \leq 0$ when $u_1 = u_2 = 0$, we need

$$[p_2 + p_3(1+kh)](a_{\rm m} + q_{\rm m}|x_2|) - \frac{k\lambda p_3^2}{-4p_2} > 0\,. \quad (4.21)$$

Since we already have the constraint $p_3 > \frac{-p_2}{1+kh}$ for the positive definiteness of P, the inequality (4.21) can be satisfied for all values of x_2 if and only if

$$a_{\rm m} > \frac{\lambda k}{(1+kh)^2}\,. \quad (4.22)$$

Returning to (4.20), we use the notation

$$c_1 = \frac{\lambda-1}{\lambda}(-p_2 k)\,,\ \ c_2 = [p_2 + p_3(1+kh)]a_{\rm m} - \frac{k\lambda p_3^2}{-4p_2}\,,\ \ c_3 = [p_2 + p_3(1+kh)]q_{\rm m}\,, \quad (4.23)$$

and completion of squares to account for the last two cross-terms:

$$\begin{aligned}\dot{V} &\leq -c_1 x_1^2 - c_2 x_2^2 - c_3|x_2|^3 - (a_{\rm m} + q_{\rm m}|x_2|)e_{\rm r}^2 \\ &\quad + p_2 x_1[u_2 - (1+kh)u_1] + x_2(p_2 u_1 + p_3 u_2) \\ &\leq -\frac{c_1}{2}x_1^2 - \frac{c_2}{2}x_2^2 - c_3|x_2|^3 - (a_{\rm m} + q_{\rm m}|x_2|)e_{\rm r}^2 \\ &\quad + \frac{p_2^2}{2c_1}[u_2 - (1+kh)u_1]^2 + \frac{1}{2c_2}(p_2 u_1 + p_3 u_2)^2\,. \quad (4.24)\end{aligned}$$

Coupled with the boundedness of $\tilde{k}_1$, $\tilde{k}_2$ and $\tilde{k}_3$, which is guaranteed by the projection in (4.17), and with the fact that $u_1 = \dot{v}_l$ and $u_2 = -kh\dot{v}_l$ are bounded and converge to zero, the inequality (4.24) proves the boundedness and regulation of x_1, x_2 and e_r. Hence, the variables v_f, v_m and δ are bounded and the vehicle following objective is achieved: $v_r \to 0$, $\delta \to 0$ as $t \to \infty$.

4.2. Autonomous operation

As shown in the previous subsection, the presented adaptive PIQ control law guarantees individual stability of the vehicles in the platoon. Now we also need to ensure string stability, i.e., attenuation of errors as they propagate upstream.

In the case of autonomous operation, the information available to each vehicle is its own velocity and the relative velocity and separation from the preceding one. If the desired intervehicle spacing is constant, i.e., $h = 0$, string stability cannot be achieved. This result is not specific to truck platoons; similar results are available for passenger cars [5, 16, 6, 2, 9]. This lack of stability is caused by the nature of propagating information in the platoon rather than by the particular vehicle dynamics.

A simple way to circumvent this problem without providing any additional information to the vehicles is to introduce a fixed time headway, i.e., $h > 0$ [5, 2], thus adding time-dependent spacing to the constant spacing. This strategy is successful in achieving string stability [5, 9] but due to the lower actuation-to-weight ratio of heavy vehicles compared to the passenger cars, the necessary minimum value of h is significantly higher and yields large intervehicle spacings at higher speeds, thereby reducing the traffic throughput.

4.3. Intervehicle communication

If the larger separation between adjacent vehicles resulting from the use of constant time headway is not acceptable, intervehicle communication can be introduced to obtain string stability with tighter spacing.

In this paper we consider the case where the lead vehicle transmits to all following vehicles in the platoon its desired speed v_d. This is a relatively simple scheme, which requires distinguishing only between the leader and the followers, who need not be aware of their sequential number in the platoon. Such a scheme was first proposed in [17], where it was shown to yield string stability for automated vehicle platoons.

In order to incorporate the new information, the difference between the platoon leader's desired speed and the current speed of the follower is defined as $v_{df} = v_d - v_f$. The control objective is modified to $v_r + k\delta + k_{df}v_{df} = 0$, where k_{df} is a tunable parameter. If we choose $k_{df} = 0$, we recover the control objective used in the autonomous operation case.

The control law is changed to reflect the new control objective:

$$u = \hat{k}_1(v_r + k\delta + k_{df}v_{df}) + \hat{k}_2 + \hat{k}_3(v_r + k\delta + k_{df}v_{df})|v_r + k\delta + k_{df}v_{df}|. \quad (4.25)$$

Similarly, the term $v_r + k\delta$ is replaced by $v_r + k\delta + k_{df}v_{df}$ in (4.8)–(4.11). Equations (4.14)–(4.22) still hold if we replace $v_r + k\delta$ by $v_r + k\delta + k_{df}v_{df}$, kh by $kh + k_{df}$, and set $u_2 = -kh\dot{v}_l + k_{df}\dot{v}_d$. As in the autonomous operation scenario, one can show that this control law guarantees $v_r \to 0$ and $\delta \to 0$.

The performed simulations confirm that using the above communication scheme guarantees string stability even for constant intervehicle spacing, i.e., for $h = 0$.

4.4. Comparative simulations

In order to compare the performance of the developed controller under different modes of operation, we simulated the behavior of a four-truck platoon using various scenarios. Profiles including acceleration and deceleration commands as well as uphill and downhill grade disturbances have been examined. The commanded profile of the simulation results presented here consists of a 4 m/s step increase of the velocity at $t = 10$ s and an 8 m/s step decrease at $t = 70$ s. We chose to present the results with this profile, because they illustrate the difficulties the system might have maintaining string stability when trying to meet a challenging acceleration/deceleration objective. In all our simulation plots, the solid lines represent the lead vehicle (Vehicle 1), while the following vehicles (Vehicles 2–4) are represented respectively with dash-dotted, dashed, and dotted lines.

One of the objectives of the simulation analysis is to investigate the effect of the time headway h on the platoon. When examining the simulation results, one should keep in mind that, while string stability is theoretically based on the separation error δ, the "vehicle separation" plot is practically more interesting as an indicator of string stability. The difference between the actual vehicle separation x_r and δ is best illustrated in Figure 8 ($h = 0.7$ s), where x_r shows a stable trend in contrast to δ, which is slightly growing as it propagates upstream from Vehicle 2 to Vehicle 4.

From the "vehicle separation" plots in Figures 7–8 we see that, in the autonomous operation case, string stability is achieved at the expense of a significant increase in intervehicle spacing. With $h = 0$ (Figure 7) the spacing is small, but the errors grow upstream. In fact, there is a near collision between the third and fourth vehicle at $t = 78$ s. The smallest headway for which x_r is stable is $h = 0.7$ s (Figure 8). This value is much larger than the $h = 0.25$ s often used for passenger cars and still may not be sufficient under different conditions. While it is expected that the lower actuation-to-weight ratio of heavy-duty vehicles will necessitate larger spacings than those used in car platoons, the spacings resulting from $h > 0.7$ s may be unacceptable.

If that is the case, the only currently available solution for reducing the spacing while guaranteeing string stability is the intervehicle communication scheme described in (4.25). As demonstrated in Figure 9, string stability is achieved with $h = 0$, which leads to a significant reduction in intervehicle

spacing, albeit at the considerable expense of introducing and maintaining communication between vehicles.

5. CONCLUSIONS

According to the AHS Precursor Systems Analysis for Commercial Vehicles and Transit [1], longitudinal control of truck platoons will be one of the most challenging problems for commercial AHS. Our research findings to date are in complete agreement with this statement and demonstrate, that longitudinal control is much more difficult for heavy-duty vehicles than for passenger cars.

Our results confirm the intuitive expectation that more aggressive control action is needed to overcome the considerably lower actuation-to-weight ratio of a heavy bus or truck compared to a passenger car and to guarantee good performance during reasonably challenging maneuvers. The usual disadvantage of passenger discomfort due to aggressive control action is much less pronounced in heavy vehicles due to their larger mass, which results in significantly lower acceleration and jerk profiles than in passenger cars.

However, simply increasing the gains of a linear controller creates a large overshoot, which is very undesirable in vehicle following. To allow fast compensation of large errors without excessive overshoot, we include nonlinear terms in our controllers, which thus outperform conventional linear controllers. We also include adaptation to make our controller response less dependent on the specific vehicle characteristics. This results in more uniform performance over a wide operating region and across non-identical vehicles, a very desirable property in platoons.

The adaptive nonlinear controller we design commands both fuel and brake, thus eliminating the need for separate fuel and brake controllers with ad hoc switching logic. Moreover, it can operate both autonomously as well as with intervehicle communication. This flexibility is desirable for two reasons:

- A vehicle equipped with this controller can take full advantage of future automated lanes, but it can also be operated in Autonomous Intelligent Cruise Control (AICC) mode in non-automated lanes.

- The AICC capability can act as a fail-safe in automated lanes, in case there is a breakdown in intervehicle communication. In the event of such a failure, the controller can simply increase the time headway and continue to operate with guaranteed string stability, albeit with lower traffic throughput.

Our results also indicate that, in the case of autonomous operation, much larger time headways are required to achieve string stability in truck platoons—at least 0.7 s, compared to 0.25 s for cars. Finally, it is worth noting that our notion of intervehicle communication includes only transmission of the *desired* speed of the leading vehicle, and can be viewed as a variation

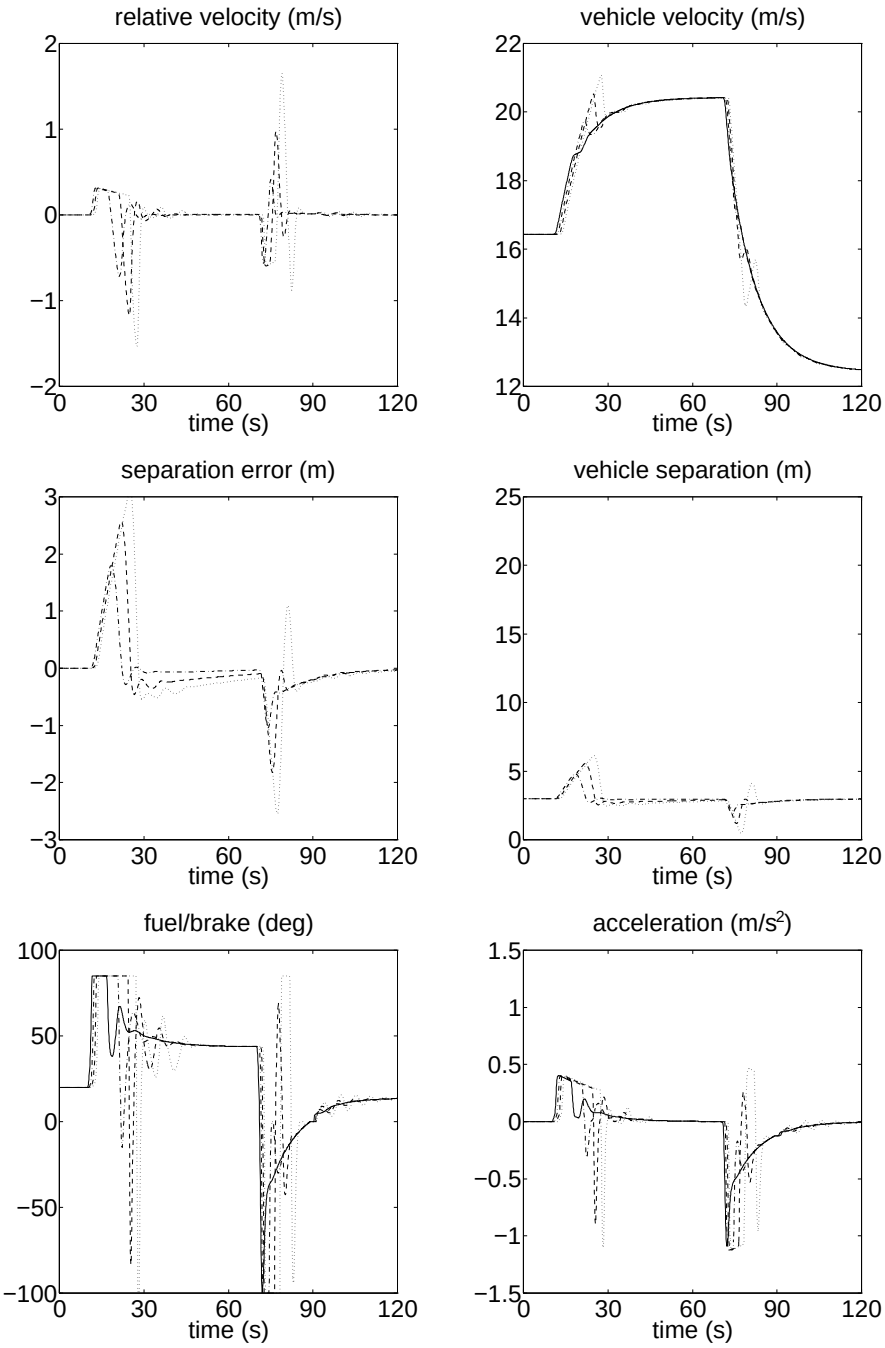

Figure 7: Autonomous operation, $h = 0$.

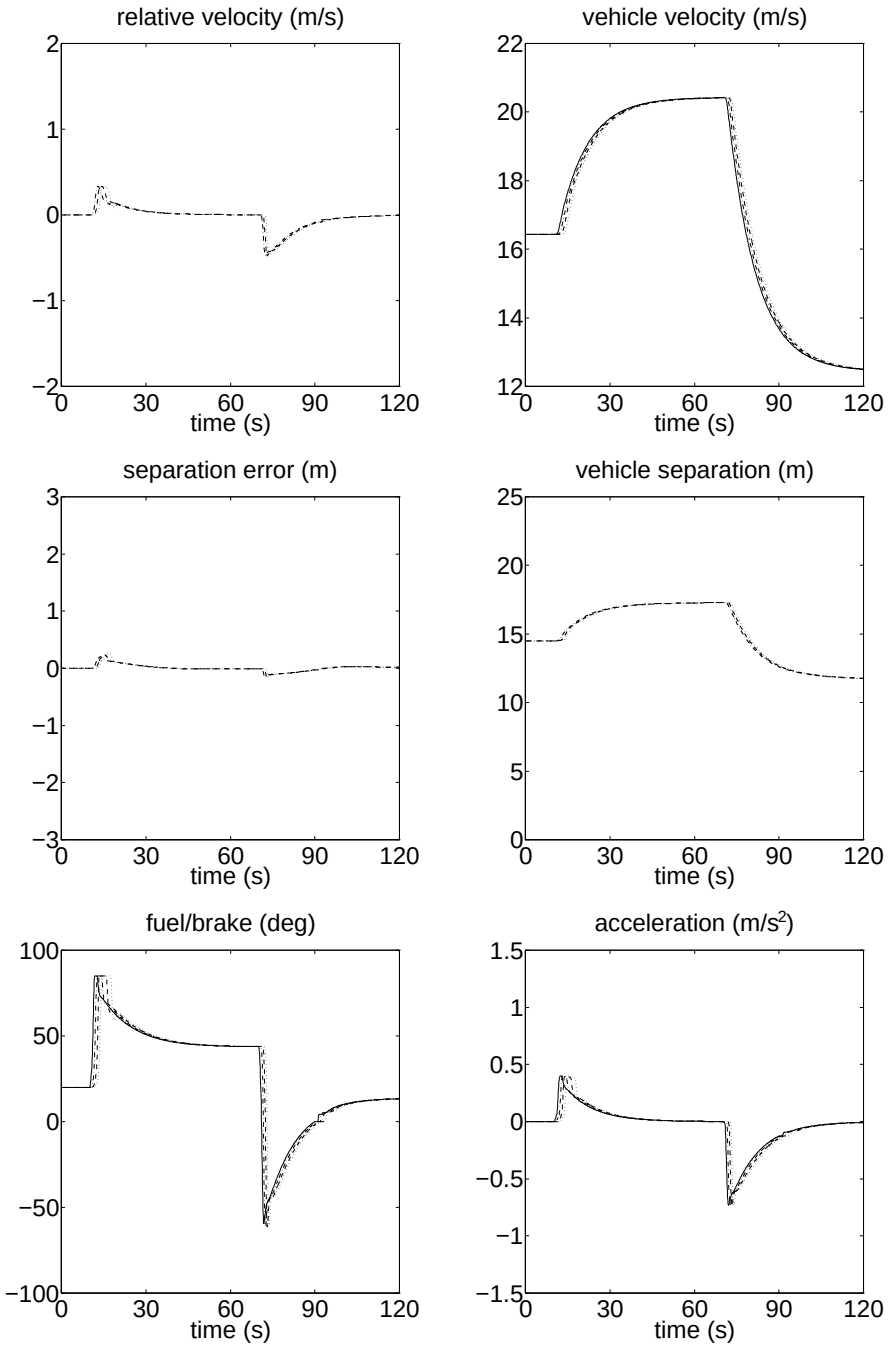

Figure 8: Autonomous operation, $h = 0.7$ s.

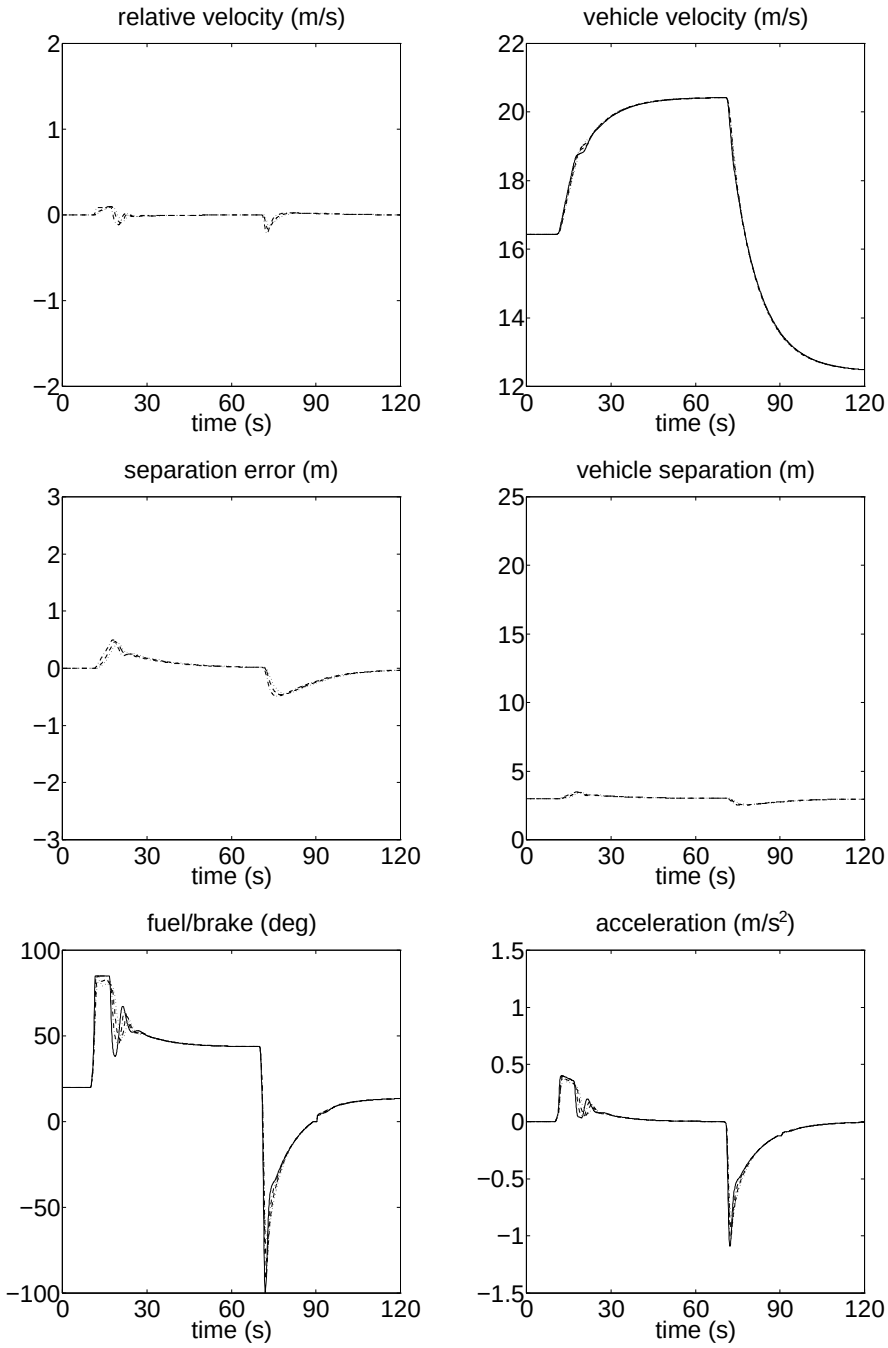

Figure 9: Intervehicle communication, $h = 0$, $k_{\mathrm{df}} = 1$.

on the approach proposed in [17]. In terms of bandwidth and reliability, this is a much less demanding scheme than the recently developed ones, which require transmission of the leader's *current speed and acceleration* in order to guarantee good performance even during very fast and demanding maneuvers.

ACKNOWLEDGMENT

This work was performed as part of the California PATH Program of the University of California, in cooperation with the State of California Business, Transportation, and Housing Agency, Department of Transportation; and the United States Department of Transportation, Federal Highway Administration.

The contents of this paper reflect the views of the authors who are responsible for the facts and the accuracy of the data presented herein. The contents do not necessarily reflect the official views or policies of the State of California. This paper does not constitute a standard, specification, or regulation.

REFERENCES

1. Bottiger, F., Chemnitz, H. D., Doorman, J., Franke, U., Zimmermann, T., and Zomotor, Z.: Commercial vehicle and transit AHS analysis. Precursor Systems Analyses of Automated Highway Systems, Final Report, vol. 6, Federal Highway Administration, Report FHWA-RD-95-XXX, 1995.

2. Chien, C. and Ioannou, P.: Automatic vehicle following. Proc. 1992 American Contr. Conf., Chicago, IL, pp. 1748–1752.

3. Cho, D. and Hedrick, J. K.: Automotive power train modeling for control. ASME J. Dyn. Sys. Meas. Contr. 111 (1989), pp. 568–576.

4. Fancher, P., Bareket, Z., and Johnson, G.: Predictive analyses of the performance of a highway control system for heavy commercial vehicles. Proc. 13th IAVSD Symposium, Supplement to Veh. Sys. Dyn. 23 (1993), pp.128–141.

5. Garrard, W. L., Caudill, R. J., Kornhauser, A. L., MacKinnon, D., and Brown, S. J.: State-of-the-art of longitudinal control of automated guideway transit vehicles. High Speed Ground Transportation Journal 12 (1978), pp. 35–68.

6. Hedrick, J. K., McMahon, D. H., Narendran, V. K., and Swaroop, D.: Longitudinal vehicle controller design for IVHS systems. Proc. 1991 American Contr. Conf., Boston, MA, pp. 3107–3112.

7. Hendricks, E.: Mean value modeling of large turbocharged two-stroke diesel engine. SAE Trans. (1989), paper no. 890564, pp. 1–10.

8. Horlock, J. H. and Winterbone, D. E.: The Thermodynamics and Gas Dynamics of Internal Combustion Engines. Claredon Press, Oxford, 1986.

9. Ioannou, P. and Xu, Z.: Throttle and brake control systems for automatic vehicle following. IVHS Journal 1 (1994), pp. 345–377.

10. Jennings, M. J., Blumberg, P. N., and Amann, R. W.: A dynamic simulation of Detroit diesel electronic control system in heavy duty truck powertrains. SAE Trans. (1986), paper no. 861959, pp. 5.943–5.966.

11. Jensen, J. P., Kristensen, A. F., Sorenson, S. C., and Hendricks, E.: Mean value modeling of a small turbocharged diesel engine. SAE Trans. (1991), paper no. 910070, pp. 1–13.

12. Kao, M. and Moskwa, J. J.: Turbocharged diesel engine modeling for nonlinear engine control and state estimation. Proceedings of the 1993 ASME Winter Annual Meeting, DSC-vol. 52, Symposium on Advanced Automotive Technologies: Advanced Engine Control Systems, New Orleans, LA.

13. Kotwicki, A. J.: Dynamic models for torque converter equipped vehicles. SAE Trans. (1982), paper no. 820393, pp. 1595–1609.

14. Ledger, J. D., Benson, R. S., and Whitehouse, N. D.: Dynamic modeling of a turbocharged diesel engine. SAE Trans. (1971), paper no. 710177, pp. 1–12.

15. McMahon, D. H., Hedrick, J. K., and Shladover, S. E.: Vehicle modeling and control for automated highway system. Proc. 1990 American Contr. Conf., San Diego, CA, pp. 297–303.

16. Sheikholeslam, S. and Desoer, C. A.: Longitudinal control of a platoon of vehicles. Proc. 1990 American Contr. Conf., San Diego, CA, pp. 291–297.

17. Shladover, S. E.: Longitudinal control of automated guideway transit vehicles within platoons. ASME J. Dyn. Sys. Meas. Contr. 100 (1978), pp. 302–310.

18. Varaiya, P.: Smart cars on smart roads: problems of control. IEEE Trans. Automat. Contr. 38 (1993), pp. 195–207.

19. Winterbone, D. E., Thiruarooran, C., and Wellstead, P. E.: A wholly dynamic model of turbocharged diesel engine for transfer function evaluation. SAE Trans. (1977), paper no. 770124, pp. 1–11.

20. Xu, Z. and Ioannou, P.: Adaptive throttle control for speed tracking. Veh. Sys. Dyn. 23 (1994), pp. 293–306.

21. Yanakiev, D. and Kanellakopoulos, I.: Engine and transmission modeling for heavy-duty vehicles. University of California, Los Angeles, California PATH Program, PATH Technical Note 95-6, 1995.

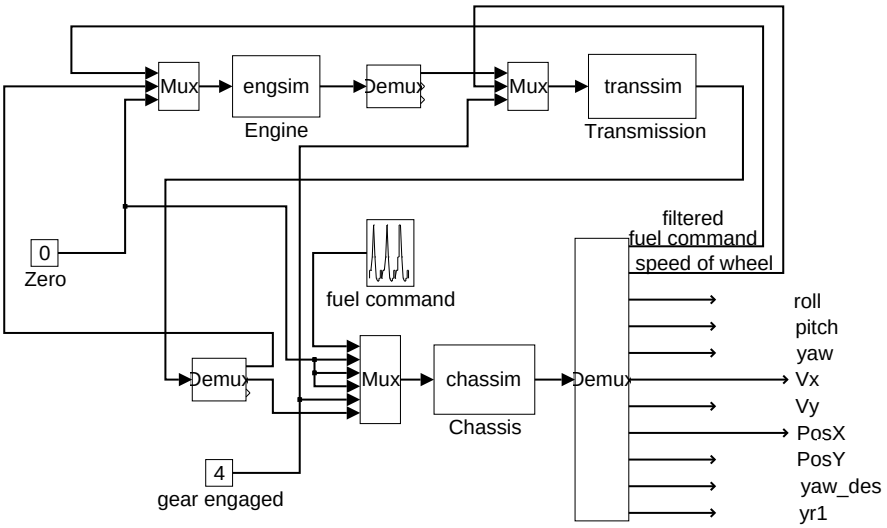

Input to Engine:	fuel command load torque unused	Output From Engine:	rpm net torque unused
Input to Trans:	rpm speed of wheel gear engaged	Ouput from Trans:	load torque driving torque unused
Input to Chassis:	commanded fuel commanded steering commanded brake road curvature gear engaged driving torque		

Figure 1: Truck longitudinal model.

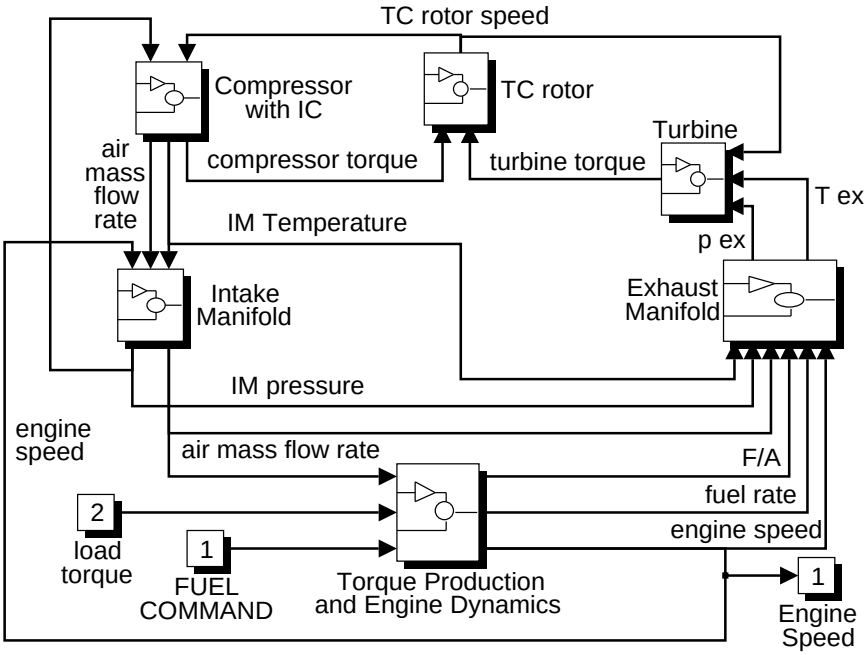

Figure 2: TC diesel engine model representation.

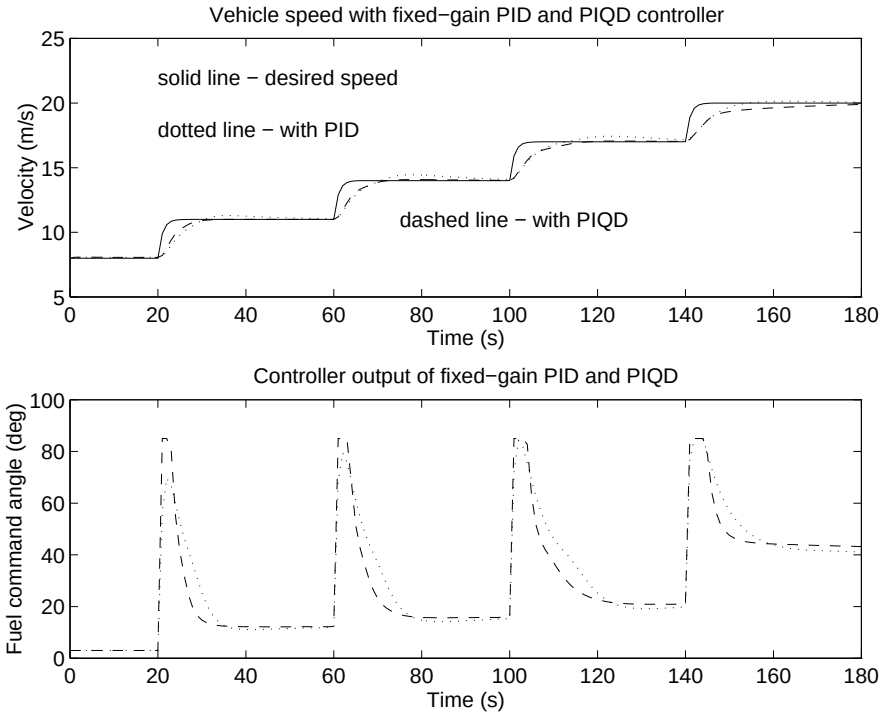

Figure 3: Vehicle speed with PID and PIQD control in response to a commanded staircase profile.

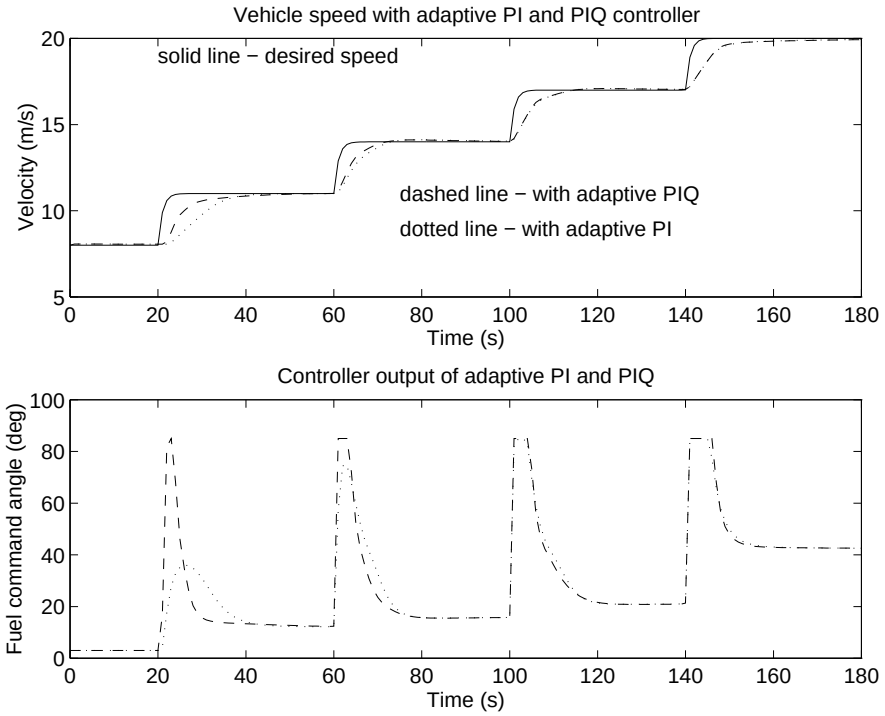

Figure 4: Vehicle speed with adaptive PI and adaptive PIQ control in response to a commanded staircase profile.

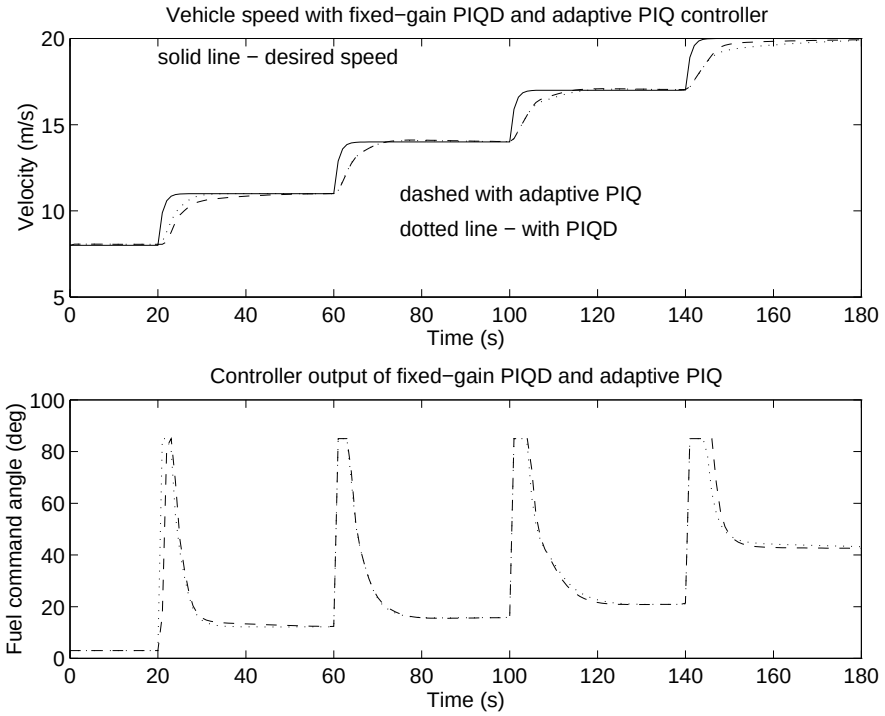

Figure 5: Performance comparison of PIQD and adaptive PIQ control.

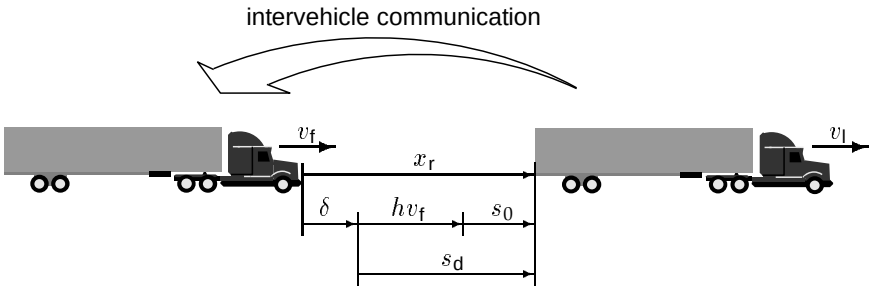

s_0 : minimum distance between vehicles
h : time headway (for speed-dependent spacing)
x_r : vehicle separation
$s_d = s_0 + hv_f$: desired vehicle separation
v_l : velocity of leading vehicle
v_f : velocity of following vehicle
$v_r = v_l - v_f$: relative vehicle velocity
$\delta = x_r - s_d$: separation error

Figure 6: Parameters of a truck platoon.

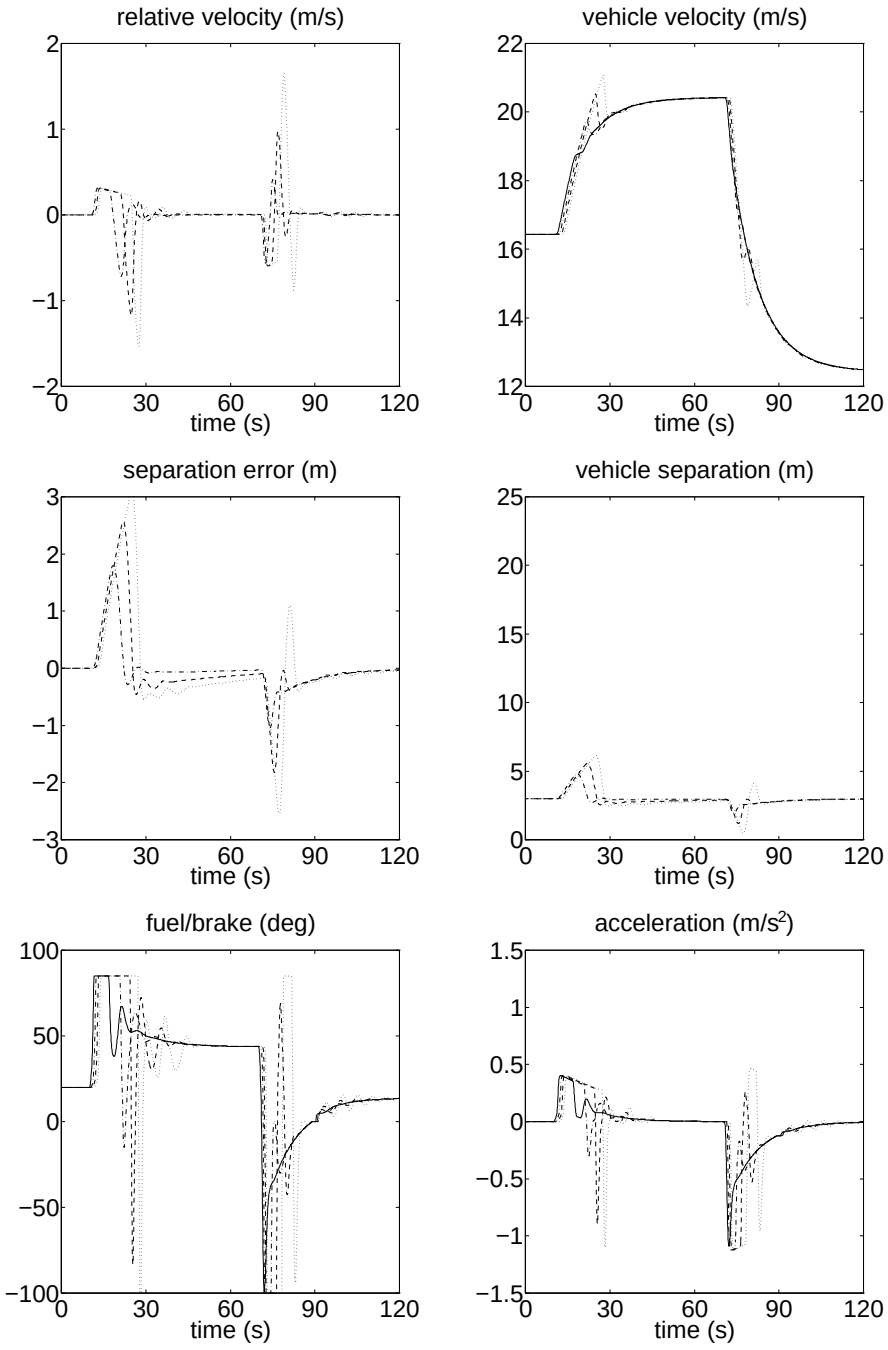

Figure 7: Autonomous operation, $h = 0$.

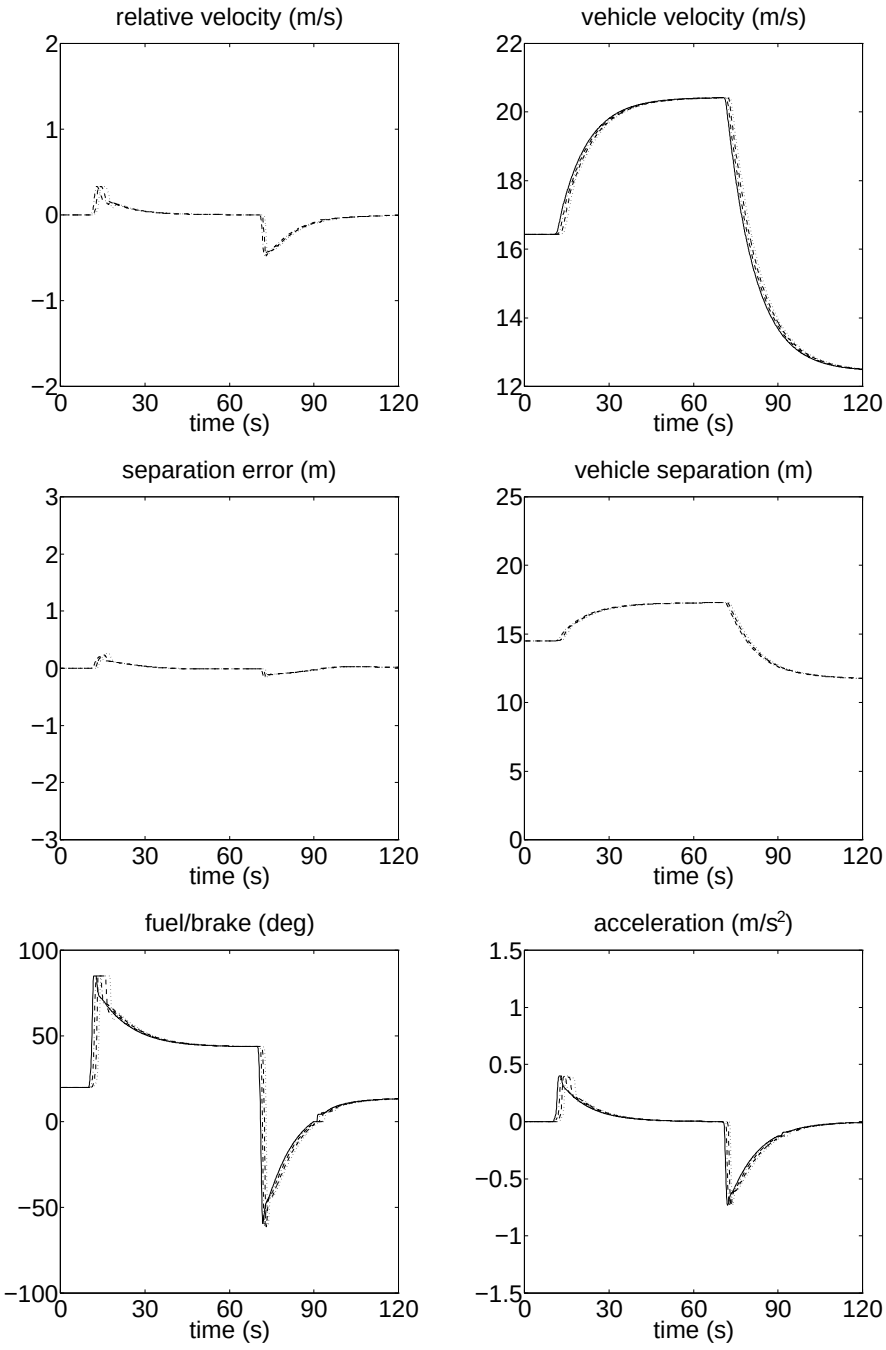

Figure 8: Autonomous operation, $h = 0.7\,\mathrm{s}$.

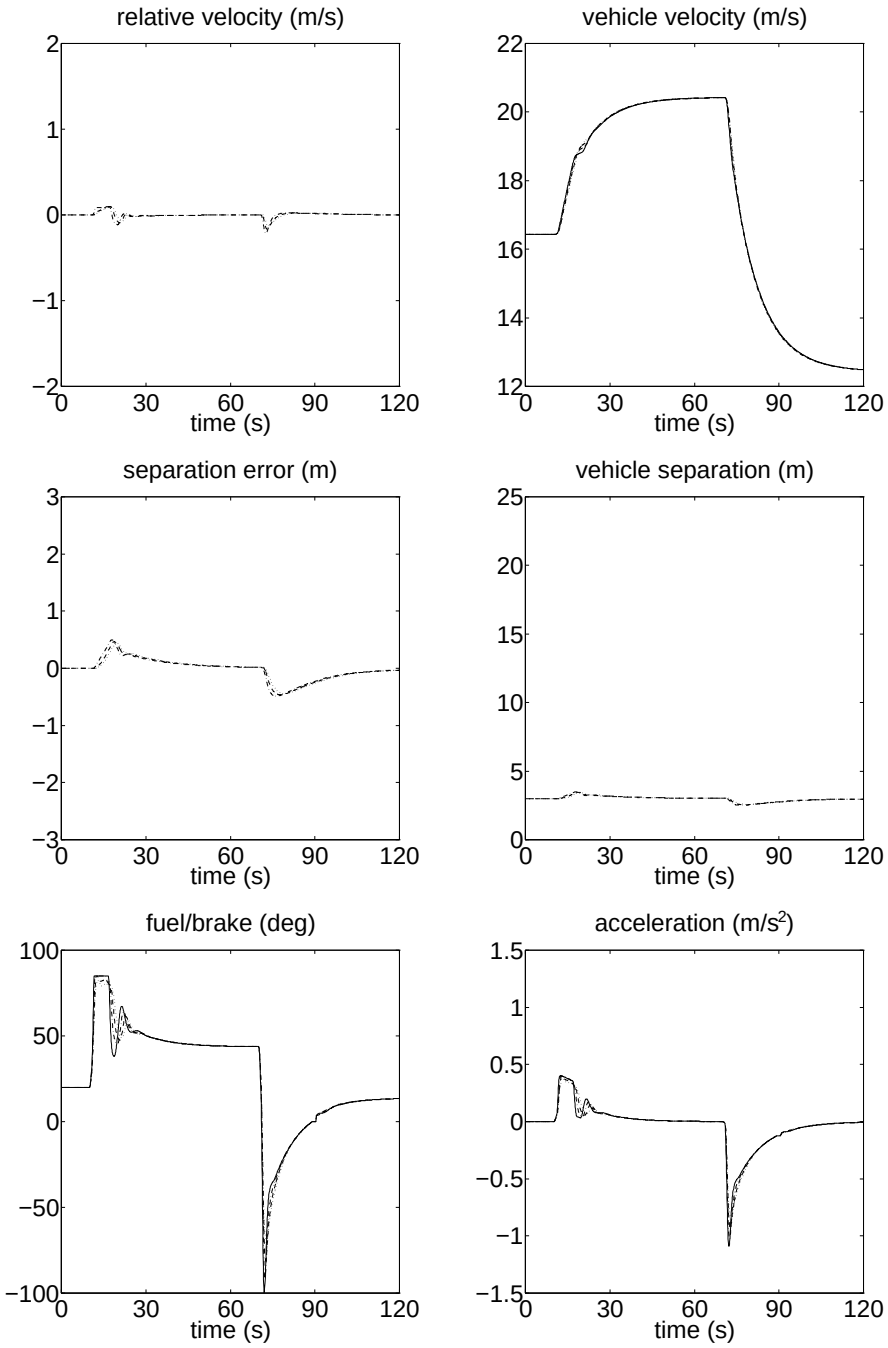

Figure 9: Intervehicle communication, $h = 0$, $k_{\mathrm{df}} = 1$.